Variation of the Axial Location of Bruch's Membrane Opening With Age, Choroidal Thickness, and Race

John Johnstone,[1] Massimo Fazio,[2] Kulawan Rojananuangnit,[2] Brandon Smith,[2] Mark Clark,[2] Crawford Downs,[2] Cynthia Owsley,[2] Michael J. A. Girard,[3,4] Jean Martial Mari,[5] and Christopher A. Girkin[2]

[1]Department of Computer and Information Sciences, College of Arts and Sciences, University of Alabama at Birmingham, Birmingham, Alabama
[2]Department of Ophthalmology, School of Medicine, University of Alabama at Birmingham, Birmingham, Alabama
[3]Department of Biomedical Engineering, National University of Singapore, Singapore
[4]Singapore Eye Research Institute, Singapore
[5]Department of Medical Physics and Bioengineering, University College London, London, United Kingdom

Correspondence: Christopher A. Girkin, 700 18th Street South, Suite 601, Birmingham, AL 35233; cgirkin@uab.edu.

Submitted: July 29, 2013
Accepted: February 23, 2014

Citation: Johnstone J, Fazio M, Rojananuangnit K, et al. Variation of the axial location of Bruch's membrane opening with age, choroidal thickness, and race. *Invest Ophthalmol Vis Sci*. 2014;55:2004–2009. DOI: 10.1167/iovs.13-12937

Purpose. This study explores variation in the axial location of Bruch's membrane opening (BMO) to determine if this reference plane varies with age and race.

Methods. There were 168 spectral-domain optical coherence tomography (SDOCT) optic nerve head volumes that were obtained from healthy subjects and manually delineated within 24 axial slices to develop point clouds for Bruch's membrane and anterior scleral surfaces. A BMO-independent reference plane was generated based on the peripapillary sclera to measure BMO position. General estimating equations were used to determine the relationship of the axial position of BMO (BMO height) with choroidal thickness, age, and race (African Descent [AD] versus European Descent [ED]) controlling for variations in axial length.

Results. The peripapillary choroid was thinner with increasing axial length (−14.9 μm/mm, $P = 0.0096$), advancing age (−1.1 μm/y, $P = 0.00091$), and in the ED group (20.2 μm, $P = 0.019$) in a multivariable model. Choroidal thickness was also strongly related to BMO height ($P < 0.00001$) independent of all covariates. Bruch's membrane opening position was more posterior relative to the sclera in older subjects (1.3 μm/y, $P = 0.00017$), independent of axial length and race. However, when choroidal thickness was included in the model, this association was lost ($P = 0.225$). There was no significant difference in BMO height between racial groups after adjustment for age and axial length.

Conclusions. Bruch's membrane opening is more posteriorly located in older individuals. These differences are largely due to differences in choroidal thickness and suggest that BMO migrates posteriorly with age due to age-related choroidal thinning. However, additional studies in longitudinal datasets are needed to validate these findings.

Keywords: optic nerve head, optical coherence tomography, choriocapillaris

Spectral-domain optical coherence tomography (SDOCT) has enabled unprecedented visualization and quantification of deep optic nerve head structures important in the development and progression of glaucomatous optic neuropathy.[1–6] Morphometric measurements of these optic nerve head structures are made based on a reference plane that has been established using the terminus of Bruch's membrane opening (BMO) at the most anterior point of the neural canal. This BMO-based reference plane allows for quantification of cup depth (based on retinal surface position), area and volume, laminar position, and prelaminar connective tissue volume.[7–10] This approach has been similarly used in histomorphometric studies of human tissues as well as animal models.[11–14] If these deep structural parameters are to be used effectively in glaucoma detection and identification of progression, understanding the effect of normal aging on BMO position is critical.

While longitudinal data is lacking, recent cross-sectional studies have demonstrated significant thinning of the choroid in the macular and peripapillary region associated with aging.[15] Given that Bruch's membrane lies on the anterior surface of the choroid, the distance between Bruch's membrane and the sclera could also decrease with age. This could lead to a posterior shift in the axial position of BMO with age as the border tissue thins in association with age-related choroidal thinning. If posterior axial migration of the BMO occurs with age, this would imply that BMO is not a stable landmark for disease progression with regards to optic disc cup, laminar, and prelaminar connective tissue depths and volumes. The purpose of this paper was to determine if BMO varies with age during adulthood and if any variance is associated with choroidal thinning.

Methods

Spectral-domain OCT data for this study were obtained from participants in two National Institutes of Health (NIH)-funded cohort studies conducted at the University of Alabama at Birmingham (UAB); the African Descent and Glaucoma

Evaluation Study (ADAGES)[16] and the Alabama Study on Early Age-Related Maculopathy study (ALSTAR). The ADAGES enrolled both individuals of African Descent (AD) and European Descent (ED), while ALSTAR enrolled only subjects of ED. Only subjects without evidence of ocular diseases that would affect the optic nerve, retina, or choroid were included, as defined below. The imaging methodologies followed in ADAGES and ALSTAR were developed to be identical. All participants gave written informed consent for both studies. The UAB institutional review board approved the study methods and these methods adhere to the tenets of the Declaration of Helsinki. Healthy subjects for both studies were recruited to join the study by advertisement and from primary eye care clinics.

Each healthy participant underwent a complete ophthalmologic exam that included medical history, Snellen best-corrected visual acuity, Early Treatment Diabetic Retinopathy Study (ETDRS) visual acuity, color vision, slit-lamp biomicroscopy, applanation tonometry, central corneal thickness (CCT) measurement (ADAGES only), axial length measurement (ADAGES only), dilated fundoscopy, stereoscopic ophthalmoscopy of the optic disc, and fundus photography. Standard SITA 24-2 perimetry was performed to define normality for inclusion in this study (see below).

Inclusion/Exclusion Criteria

All participants were over 18 years of age for the ADAGES study and over 60 for the ALSTAR study. Eligible participants had open angles, a best corrected acuity of 20/40 or better, and refractive error up to 5.0 diopters (D)-sphere and 3.0-D cylinder. Patients with diabetes and any retinal, corneal, or optic nerve disease were excluded. A family history of glaucoma was allowed. Participants were excluded if they had a history of intraocular surgery (except for uncomplicated cataract surgery), elevated IOP (>22) at the time of the study, a history of elevated IOP, prior use of glaucoma medication, other intraocular eye disease, other diseases affecting visual field (e.g., pituitary lesions, demyelinating diseases, HIV+, or AIDS). Further, patients were excluded if there was a diagnosis of Alzheimer's disease, Parkinson's disease, or previous brain injury including stroke, psychoses, or other neurologic or psychiatric conditions that would prevent participation in a psychophysical test.

We required a reliable test on 24-2 standard automated perimetry (SAP; Carl Zeiss Meditec, Dublin, CA) using the Swedish Interactive Thresholding Strategy (SITA) in both eyes at baseline for inclusion in the study. Reliability was defined as less than 33% false positives, false negatives, and fixation losses. A field was considered normal if the pattern standard deviation (PSD) was not triggered at 5% or less and the Glaucoma Hemifield Test (GHT) were within normal limits and the field showed no sign of glaucomatous defect based on subjective evaluation from the enrolling clinician. The optic nerves were assessed by stereo photos by a fellowship-trained glaucoma specialist (CAG). Subjects with any structural finding suggestive of glaucoma (i.e., notching, rim thinning, disc hemorrhages, or retinal nerve fiber layer defects as judged) were excluded.

SDOCT Image Acquisition, Processing, and Quantification

All subjects underwent SDOCT imaging with the Spectralis OCT (Family Acquisition Module 5.4.8.0; Heidelberg Engineering GmbH, Heidelberg, Germany) with 48, 20° radial scans centered on the center of the optic nerve head using enhanced depth imaging (EDI).[6] Scans were evaluated for imaging quality by the operator and images were re-acquired if there was improper B-scan positioning in the imaging frame, a quality score less than 20, or poor centration of the optic nerve head. A total of 168 scans from both eyes of 84 study subjects were included. Radial scans were constructed from an average of 9 ($n = 108$) or 12 ($n = 60$) scans/slice using the instrument's internal software. Nine scans were averaged in the ADAGES protocol and 12 scans were averaged in the ALSTAR protocol. All other characteristics of the imaging protocols were identical. There were no differences in any of the morphometric parameters obtained related to the different averaging protocols.

In order to correct the deleterious effects of light attenuation observed in OCT images, all B-Scans from all OCT volumes were post processed using adaptive compensation with a threshold exponent of 2.[17] This algorithm has been demonstrated (1) to significantly increase the interlayer contrast (a measure of tissue boundary visibility) across all major optic nerve head tissue boundaries, (2) to significantly reduce the intralayer contrast (a measure of blood vessel shadow visibility) within all tissues, (3) to improve the visibility of lamina cribrosa insertions and focal laminar defects in some cases, and to (4) remove noise overamplification in the deepest tissue layers.

Radial SDOCT scan volumes were loaded and aligned in custom software developed for three-dimensional delineation of histologic and OCT data that has been described in prior publications[10,11] based on the Visualization Toolkit (VTK; Kitware, Inc., Clifton Park, NY). A trained observer masked to subject characteristics manually delineated 24 equally spaced radial sections. Principal surfaces delineated included: retinal surface, Bruch's membrane surface, scleral surface, and anterior surface of the lamina cribrosa (Fig. 1). The Bruch's membrane surface and scleral surface were used for all further analysis in this study to define the BMO, BMO plane, scleral reference region, BMO height, and choroidal thickness, as described below. Two eyes were eliminated due to inadequate visualization of the anterior sclera following compensation.

The BMO was defined as the inner boundary of the Bruch's membrane (i.e., the boundary nearer to the rotational axis. The BMO plane was defined as the best-fitting plane of the BMO (which happens to be pseudoplanar), using principal component analysis as follows. A plane is defined by its normal and a point on the plane. If B is the BMO point cloud (the inner boundary points of all 24 Bruch's membrane sections) and C is the covariance matrix of B, the normal of the BMO plane is the eigenvector of C associated with the smallest eigenvalue, and a point on the BMO plane is the mean of B.[18]

The center of the BMO was defined as the center of its best-fitting ellipse, which, like the BMO plane, can be computed by principal component analysis. The scleral reference region was defined as the anterior scleral surface located between 1700 and 1800 μm from the BMO axis, the line through the center of the BMO and orthogonal to the BMO plane. This region was chosen, since the scleral surface seemed most visible in this region when reviewing the scan data. The scleral reference position for each section was defined as the mean surface position of the scleral reference region as defined above. An average measure of scleral position over a 100-μm region was chosen to avoid any errors due to focal perturbations of the scleral surface shape and minimize the error associated with inaccurate definition of the position of the BMO central axis. The BMO height of a section was defined as the distance from the BMO plane to the scleral reference position within that section, and the overall BMO height was defined as the mean of the BMO heights of each section. The BMO height allows for the evaluation of changes in axial position of the BMO with demographic and ocular variables relative to a peripheral scleral reference point away from the neural canal.

Investigative Ophthalmology & Visual Science

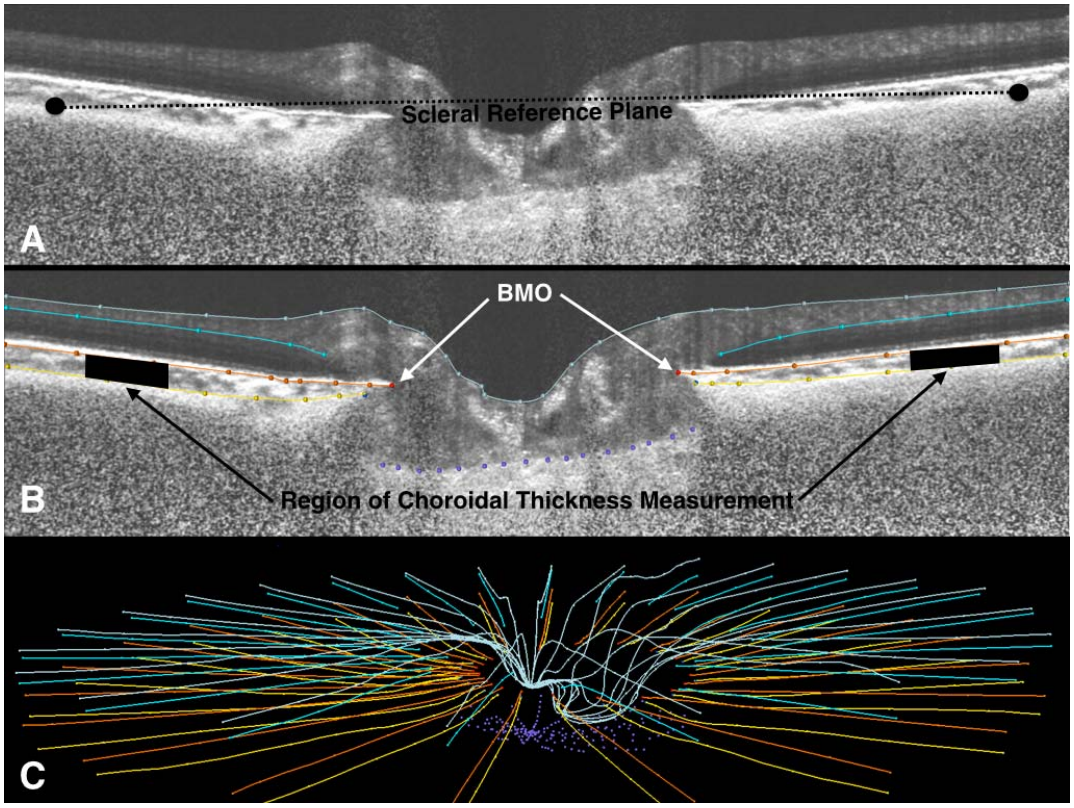

Figure 1. (**A**) Representative radial section from a compensated SDOCT of the optic nerve head showing the location of placement of the scleral reference plane based on the average position of the scleral between 1700 and 1800 μm from BMO. (**B**) Principal surfaces delineated and delineation marks within a sample SDOCT radial section. Only Bruch's membrane surface (*orange lines* and *marks*) and anterior scleral surface (*yellow lines* and *marks*) were used for this study. The region of measurement of choroidal thickness is illustrated and is located 1000 to 1500 μm from BMO. (**C**) Visualization of complete delineated surfaces. Anterior scleral surface is in *yellow* and Bruch's membrane is in *orange*.

Choroidal thickness was defined as the distance between the Bruch's membrane and the anterior sclera, measured along a normal to Bruch's membrane. Since Bruch's membrane exhibits local irregularities, yet each section of Bruch's membrane is pseudolinear, it is more robust to replace each section of Bruch's membrane by a line for the purposes of computing the normal of Bruch's membrane. This thickness is sampled along Bruch's membrane between 1000 and 1500 μm away from the BMO, and the mean of these thicknesses is used as the overall choroidal thickness. This location was chosen because the anterior scleral surface is difficult to visualize (and thus to define accurately) in regions more adjacent to the border of the neural canal, due to shadowing from the retinal vessels and reduced signal intensity from thick overlying tissues.

We initially attempted to measure the choroid directly adjacent (100–150 μm) to BMO. However, these measurements showed poorer correlations to axial length. Investigating this unexpected result, we found that for all associations (i.e., age, axial length, and BMO height), the correlations with choroidal thickness increased moving away from BMO. Given that all the variables are showing the same effect, this is likely due to higher measurement variability adjacent to the nerve head. This effect leveled from 1000 to 1500 μm, which is why this regions was selected. Further, this is a similar location measured by other studies that have examined the peripapillary choroid.[19,20]

Analysis

The BMO height variation with age, race, and choroidal thickness was analyzed by means of general estimating equations (geeglm, *R* package 3.0.0; Foundation for Statistical Computing, Vienna, Austria); the statistical model accounted for correlation among fellow eyes from the same individual. Full models were constructed using significantly associated variables, which included age, race, axial length, and choroidal thickness as independent variables and BMO height as the dependent variable. Models were run with and without choroidal thickness to determine the effects of this parameter on the associations with BMO height with age and race. Associations between choroidal thickness with race, age, and axial length were also investigated in similar modelling procedures.

Results

Demographic and ocular characteristics are described in Table 1 and compared across racial groups. The AD group was significantly younger that the ED group. The axial length was shorter in the AD group, but this did not reach statistical

Table 1. Demographic and Ocular Characteristics

Parameter	African Descent Mean (SD)	European Descent Mean (SD)	*P*
Age	42.9 (10.1)	60.8 (17.8)	<0.0001
Axial length	23.7 (0.8)	23.9 (0.7)	0.29
IOP	15.1 (2.9)	14.4 (2.5)	0.11
Spherical equivalent	−0.8 (1.3)	−0.5 (2.0)	0.22

Investigative Ophthalmology & Visual Science

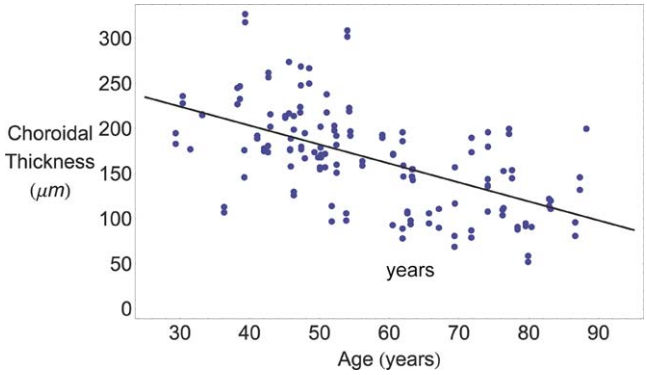

Figure 2. Scatterplot and regression line of choroidal thickness and age. Regression line: Choroidal thickness = 288 − 2.11 × age. Slope adjusted for race and axial length = −1.1 μm/y ($P = 0.00091$).

significance. In the multivariable model choroidal thickness was independently associated with age (−1.1 μm/y; $P = 0.00091$), axial length (−14.9 μm/mm, $P = 0.0096$), race (20.2 μm thicker in the AD group, $P = 0.019$) and BMO height ($P < 0.00001$) with a thinner choroid associated with advancing age, longer axial length, and a more posterior BMO height. The scatterplots for the association between choroidal thickness with age and BMO height are shown in Figures 2 and 3, respectively.

Table 2 shows the results of the multivariable model with BMO height as the dependent variable. Model 1, which includes age, race, and axial length, shows a significant association with age, independent of axial length and race. The crude data is shown in the scatterplot for association between age and BMO height in Figure 4. There is a mean reduction of −1.3 μm/y in this model ($P = 0.0017$). However, in Model 2, in which choroidal thickness is included, this association is no longer present and choroidal thinning is strongly correlated to lower BMO height, suggesting that much of the posterior shift in BMO position related to increased age may be driven by choroidal thinning that was strongly associated with age (Fig. 2).

While no difference in BMO height were observed between the AD and ED group following adjustment for axial length and age, the AD group had a greater age-related reduction in BMO height than the ED group (AD: −2.5 μm/y, $P < 0.00001$; ED: −0.8 μm/y, $P = 0.035$). When choroidal thickness was added to the model the association between age and BMO height was

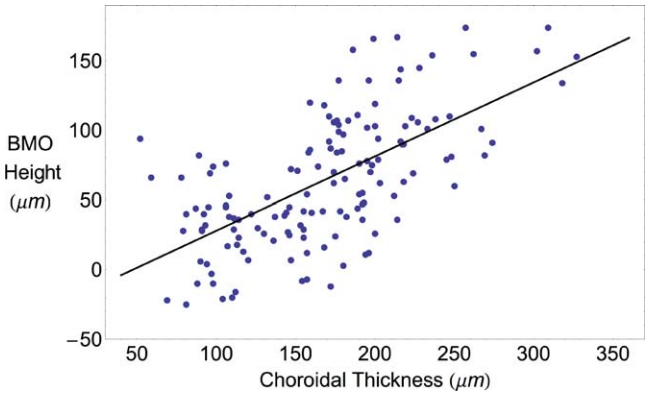

Figure 3. Scatterplot and regression line BMO height and choroidal thickness. Regression line: BMO Height = −25.1 + 0.53 × choroidal thickness. Slope adjusted for age, race, and axial length = + 0.48 μm/y ($P = <0.0001$).

Table 2. Estimates and Associated *P* Values for the Partial and Full Multivariable Models

	Model 1		Model 2	
Coefficients	**Estimate**	***P***	**Estimate**	***P***
Race	11.9	0.21	−1.3	0.87
Age	−1.3	0.00017	−0.4	0.2252
Axial length	10.7	0.025	14.9	0.0021
Choroidal thickness	Excluded		0.48	0.00000005

Model 1: BMO Height ~ Race + Age + Axial length. Model 2: BMO Height ~ Race + Age + Axial Length + Choroidal thickness.

greatly reduced but remained significant only in the AD group (AD: −1.3 μm/y, $P < 0.0058$; ED: −0.1 μm/y, $P = 0.6557$).

Discussion

This study demonstrated a significant association between age and the axial position of BMO, with BMO located more posteriorly in older individuals. This more posterior BMO position was also associated with an observed thinning of the choroid that occurred with aging. This implies that as the choroid thins with age, BMO position shifts more posteriorly. This finding has important ramifications for the quantification of deep optic nerve structure since measurements of laminar and prelaminar tissue positions are based on a BMO-based reference plane. To the best of our knowledge, this is the first study examining the association of the BMO reference plane as defined by SDOCT with age.

The BMO-based measurements have been used with SDOCT and with morphometric quantification of histologic reconstructions. Our findings would not likely affect measurement of structures anterior to BMO such as the recently developed minimum rim distance approach,[7] but should have significant effect on cup depth, laminar depth, prelaminar tissue volume, along with measurements of cup area and volume, rim area and volume, and cup-to-disc ratio. Further work using a scleral-based reference plane will be important to explore these differences both for cross-sectional detection studies and longitudinal progression studies.

Since choroidal thinning with age is associated with the posterior migration of BMO, it is likely that the border tissue that lies between the anterior scleral canal and BMO also shortening with age, drawing BMO closer to the anterior scleral canal opening. Another alternative is that BMO and

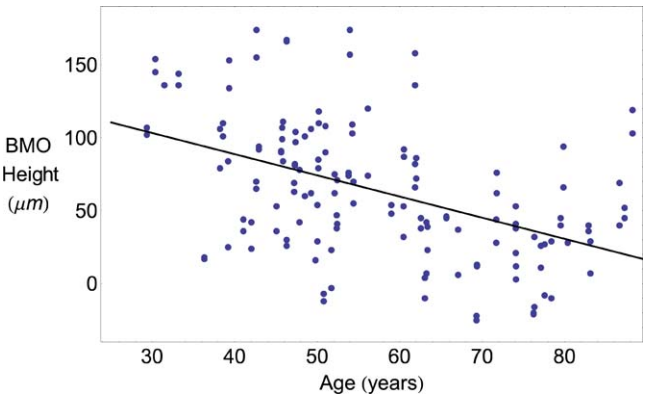

Figure 4. Scatterplot and regression line BMO height and age. Regression line: BMO Height = 147 − 1.45 × age. Slope adjusted for axial length and race = −1.3 ($P = 0.00017$).

Investigative Ophthalmology & Visual Science

anterior scleral canal opening both migrate as a unit with increased posterior bowing of the tissue just adjacent to the neural canal with age. Since it is difficult to accurately identify anterior scleral canal opening in SDOCT data, this study cannot differentiate between these two possibilities and histologic data would be more useful to explore this further.

It is interesting that there appears to be a stronger age-related association with reduction in BMO height in the AD group than in the ED group and that the association within the AD group persists following adjustment for choroidal thickness. This suggests that not all of the posterior shift in BMO position can be explained by thinning of the choroid in the AD group. However, given the sample size and age differential across racial groups, this finding should be interpreted with caution and additional work is needed to clarify any association.

While choroidal thickness in the macula has been well studied, only two studies have examined choroidal thickness in the peripappillary region in healthy subjects and presented correlations with age and axial length. Roberts and coworkers,[20] using a 12° circle scan obtained from 92 healthy participants, found that choroidal thickness decreased by approximately 1.1 μm/y ($P < 0.001$) and by 10 μm/mm increase in axial length ($P = 0.04$). These results are quite similar to the ones in this study (advancing age −1.1 μm/y; axial Length −14.9 μm/mm). Huang and coworkers[19] used a similar scan pattern in 76 healthy Chinese volunteers to evaluate choroidal thickness and found a similar association with age (−1.33 μm/y), but conversely no significant associations with axial length, IOP, or blood pressure.

This study is limited due to its cross-sectional nature to only show associations between aging, choroidal thinning, and posterior migration of the BMO. While the strong association between aging and posterior migration of the BMO is suggestive that this landmark may not provide a stable reference plane, further research using longitudinal data would be needed to determine estimates of rates of change with age and to validate these findings. Further, the study sample size is relatively small, but similar to the existing literature on normal peripappillary choroidal thickness. However the strong associations demonstrated in the models suggest that the study is adequately powered to estimate these particular associations. Additionally, this study only included healthy subjects, as the focus of this investigation was to study normal aging. These differences may be greater in subjects with glaucoma, in which atrophy of the choroid surrounding the nerve is common,[21,22] assuming thinning occurs in association with overt atrophy.

Additional limitations include the lack of use of EDI for this study, which used data from two studies developed prior to the widespread use of EDI imaging. However, the use of the adaptive compensation algorithms enhanced the visualization of the anterior sclera. Further, we did not time the imaging with the cardiac cycle, which could have some effect on the thickness measurements of the choroid. However, since the image clarity is unlikely to differ with age or across race and any cardiac cycle timing effect would be completely random, both of these limitations would be nondifferential with respect to age and race, and thus would have biased result away from significance. Since we found several highly significant associations this is not an issues other than our study may underestimate these associations to some degree. Lastly, while a scleral-based reference plane will not have the issues related to age-related choroidal thinning, changes in sclera may still occur with age and in glaucoma that could also impact this approach as well.

In summary, the current study demonstrated a significant posterior shift in the axial position of BMO associated with increasing age. These results imply that a BMO-based reference plane may not be stable and calls into question the use of this reference plane in the quantification of optic nerve parameters. An alternative reference plane based on the visualized peripapillary sclera may be useful in optic disc morphometric measures, but further evaluation is needed especially in longitudinal datasets.

Acknowledgments

The authors thank Claude Burgoyne, MD, for his assistance and the Optic Nerve Head Research Laboratory of the Devers Eye Institute for providing the Multiview delineation software use in this study.

Supported by grants from the National Eye Institute (EY018926, EY14267, and EY019869) the National Institute on Ageing (R01AG04212), the Eyesight Foundation of Alabama, Research to Prevent Blindness, and the Singapore Ministry of Education, Academic Research Fund, Tier 1.

Disclosure: **J. Johnstone**, None; **M. Fazio**, None; **K. Rojananuangnit**, None; **B. Smith**, None; **M. Clark**, None; **C. Downs**, None; **C. Owsley**, None; **M.J.A. Girard**, None; **J.M. Mari**, None; **C.A. Girkin**, None

References

1. You JY, Park SC, Su D, Teng CC, Liebmann JM, Ritch R. Focal lamina cribrosa defects associated with glaucomatous rim thinning and acquired pits. *JAMA Ophthalmol*. 2013;131:314–320.
2. Park SC, Kiumehr S, Teng CC, Tello C, Liebmann JM, Ritch R. Horizontal central ridge of the lamina cribrosa and regional differences in laminar insertion in healthy subjects. *Invest Ophthalmol Vis Sci*. 2012;53:1610–1616.
3. Yang H, Qi J, Hardin C, et al. Spectral-domain optical coherence tomography enhanced depth imaging of the normal and glaucomatous nonhuman primate optic nerve head. *Invest Ophthalmol Vis Sci*. 2012;53:394–405.
4. Park HY, Jeon SH, Park CK. Enhanced depth imaging detects lamina cribrosa thickness differences in normal tension glaucoma and primary open-angle glaucoma. *Ophthalmology*. 2012;119:10–20.
5. Park SC, De Moraes CG, Teng CC, Tello C, Liebmann JM, Ritch R. Enhanced depth imaging optical coherence tomography of deep optic nerve complex structures in glaucoma. *Ophthalmology*. 2012;119:3–9.
6. Lee EJ, Kim TW, Weinreb RN, Park KH, Kim SH, Kim DM. Visualization of the lamina cribrosa using enhanced depth imaging spectral-domain optical coherence tomography. *Am J Ophthalmol*. 2011;152:87–95, e81.
7. Chauhan BC, O'Leary N, Almobarak FA, et al. Enhanced detection of open-angle glaucoma with an anatomically accurate optical coherence tomography-derived neuroretinal rim parameter. *Ophthalmology*. 2013;120:535–543.
8. Reis AS, O'Leary N, Yang H, et al. Influence of clinically invisible, but optical coherence tomography detected, optic disc margin anatomy on neuroretinal rim evaluation. *Invest Ophthalmol Vis Sci*. 2012;53:1852–1860.
9. Reis AS, Sharpe GP, Yang H, Nicolela MT, Burgoyne CF, Chauhan BC. Optic disc margin anatomy in patients with glaucoma and normal controls with spectral domain optical coherence tomography. *Ophthalmology*. 2012;119:738–747.
10. Strouthidis NG, Yang H, Downs JC, Burgoyne CF. Comparison of clinical and three-dimensional histomorphometric optic disc margin anatomy. *Invest Ophthalmol Vis Sci*. 2009;50:2165–2174.
11. Downs JC, Yang H, Girkin C, et al. Three-dimensional histomorphometry of the normal and early glaucomatous monkey optic nerve head: neural canal and subarachnoid

space architecture. *Invest Ophthalmol Vis Sci*. 2007;48:3195–3208.

12. Fortune B, Choe TE, Reynaud J, et al. Deformation of the rodent optic nerve head and peripapillary structures during acute intraocular pressure elevation. *Invest Ophthalmol Vis Sci*. 2011;52:6651–6661.
13. Yang H, Downs JC, Bellezza A, Thompson H, Burgoyne CF. 3-D histomorphometry of the normal and early glaucomatous monkey optic nerve head: prelaminar neural tissues and cupping. *Invest Ophthalmol Vis Sci*. 2007;48:5068–5084.
14. Yang H, Downs JC, Girkin C, et al. 3-D histomorphometry of the normal and early glaucomatous monkey optic nerve head: lamina cribrosa and peripapillary scleral position and thickness. *Invest Ophthalmol Vis Sci*. 2007;48:4597–4607.
15. Barteselli G, Chhablani J, El-Emam S, et al. Choroidal volume variations with age, axial length, and sex in healthy subjects: a three-dimensional analysis. *Ophthalmology*. 2012;119:2572–2578.
16. Sample PA, Girkin CA, Zangwill LM, et al. The African Descent and Glaucoma Evaluation Study (ADAGES): design and baseline data. *Arch Ophthalmol*. 2009;127:1136–1145.
17. Girard MJ, Strouthidis NG, Ethier CR, Mari JM. Shadow removal and contrast enhancement in optical coherence tomography images of the human optic nerve head. *Invest Ophthalmol Vis Sci*. 2011;52:7738–7748.
18. Hughes H, DeRose T, Duchamp T, McDonald J, Stuetzle W. Surface reconstruction from unorganized points. *ACM SIGGRAPH*. 1992;26:71–78.
19. Huang W, Wang W, Zhou M, et al. Peripapillary choroidal thickness in healthy Chinese subjects. *BMC Ophthalmol*. 2013;13:23.
20. Roberts KF, Artes PH, O'Leary N, et al. Peripapillary choroidal thickness in healthy controls and patients with focal, diffuse, and sclerotic glaucomatous optic disc damage. *Arch Ophthalmol*. 2012;130:980–986.
21. Teng CC, De Moraes CG, Prata TS, et al. The region of largest beta-zone parapapillary atrophy area predicts the location of most rapid visual field progression. *Ophthalmology*. 2011;118:2409–2413.
22. Jonas JB, Naumann GO. Parapapillary chorioretinal atrophy in normal and glaucoma eyes. II. Correlations. *Invest Ophthalmol Vis Sci*. 1989;30:919–926.

Investigative Ophthalmology & Visual Science